NJC

New Journal of Chemistry

A journal for new directions in chemistry

Accepted Manuscript

NJC

New Journal of Chemistry

A journal for new directions in chemistry

rsc.li/njc

Volume 42
Number 6
21 March 2018
Pages 3963-4776

ISSN 1144-2546

PAPER
Chechia Hu, Tzu-Jen Lin *et al*
Yellowish and blue luminescent graphene oxide quantum dots prepared via a microwave-assisted hydrothermal route using H2O2 and KMnO4 as oxidizing agents

ROYAL SOCIETY OF CHEMISTRY

cnrs

ROYAL SOCIETY OF CHEMISTRY

rsc.li/njc

Bioinspired catalysis and Bromoperoxidase like activity of Multistimuli-Responsive Supramolecular Metallogel: Supramolecular assembly triggered by pi-pi stacking and hydrogen bonding interactions

Sunshine Dominic Kurbah and Ram A. Lal

Centre for Advanced Studies, Department of Chemistry, North-Eastern Hill University, Shillong-793022, India.

ABSTRACT

We report the synthesis and characterization of new self-assemble VO_2-L metallogel. Gel formation was investigated by dissolving VO_2-L in various solvents and it was found that water/methanol (1:9 (v/v) ratios) induces gel formation. Single X-ray crystal structure of VO_2-L metallogel exhibits C-H---O, N-H---O hydrogen bonding interaction and pi-pi stacking. The VO_2-L Xerogel obtained after removing the solvents were found to exhibit outstanding performance in catalysis. Bromoperoxidase-like activity of VO_2-L metallogel was also reported. The present catalytic studies are simple and proceed under mild condition.

Keywords: Pi-pi stacking, metallogel, catalysis and bromoperoxidase

INTRODUCTION

Oxidative bromination of organic molecules constitutes one of the most important and fundamental research in organic chemistry, because of its precursors for various transformations employed in organic and pharmaceutical synthesis [1-3]. Conventional method for bromination of organic substrates utilized toxic and hazardous elemental bromine, which is both health hazard and harmful from environmental point of view, in which half of the bromine ends up as hydrogen bromide wastes [4-6]. Alternative safer method for oxidative bromination which are less harmful and toxic can be developed by using suitable brominating agents such as, N-bromoacetamide (NBA), N-bromosuccinimide (NBS), or bromodimethylsulfonium bromide [7, 8]. However, these protocols find many drawbacks due to high cost and generation of organic waste associated with these reagents. However, re-oxidation of HBr using hydrogen peroxide can solve this problem.

Hence, for developing new and efficient method that are environmentally and economically favorable, efforts have been made using bromide ion as a bromide source instead of bromine. Using various oxidants such as hydrogen peroxide [9, 10], cerium ammonium nitrate [11, 12], oxone [13], lead tetra-acetate [14], and sodium periodate [15, 16] in presence of tetrabutylammonium bromide or alkali metal bromide has been shown to

enhance the oxidative bromination. Additionally, mimicking bromination reaction of a naturally occurring enzyme vanadium bromoperoxidase found in marine algae has attracted much attention in the past years [17-19]. In the presence of H_2O_2, bromoperoxidase catalyzes two-electron oxidation of bromide ion, forming a bromonium-like species, which induces the bromination of organic compounds [20, 21]. Metals like vanadium [22-24], tungsten [25], molybdenum [26] and rhenium [27] have been used as a bromination catalyst in the presence of stoichiometric amount of hydrogen peroxide. On the other hand, using molecular oxygen as a terminal oxidant in place of a strong oxidant have been reported by few groups by developing the more advanced catalytic systems rather than the enzyme for bromination reactions [28, 29].

Furthermore, supramolecular gels have potential applications in catalysis [30]. Moreover, when the catalyst is immobilised within the network, the reagents can diffuse into gels, whereas the products diffuse out. Supramolecular gels can also provide catalyst longevity, protection from product contamination and easy separation [30]. Hence, it has been challenges to design and develop a simple catalytic system that can both remediate waste, and subsequently act as active catalysts. In this paper, we report the oxidative bromination of some organic substrate using newly synthesized VO_2-L metallogel derived from hydrazone ligand in presence of hydrogen peroxide.

EXPERIMENTAL METHODS

Materials

Solvents were reagents grade purchased from Himedia. Other chemicals such as aniline, acetophenone, 2-nitrophenol, 2-hydroxyacetophenone, 2-hydroxybenzaldehyde, 4-methoxyacetophenone, 2-hydroxyethylbenzoate, 3-methylacetophenone, 4-methylacetophenone and 4-chlorophenol were purchased from Sigma Aldrich and were used as received without any further purification. Vanadium pentoxide and other metal salts were purchased from Himedia and were used as received.

Single X-ray crystallography

Single crystal X-ray data were collected at 291.8 K, using Xcalibur, Eos, Gemini diffractometer equipped with a monochromated Mo K radiation ((λ = 0.71073 Å). The CrysAlis PRO; Agilent, 2013 software packages were used for data collection and reduction. The intensity data were corrected using semi empirical absorption method. In all cases absorption corrections based on multiscan using SADABS software were applied [31]. The crystal structure was solved and refined using SHELXL-2014 [32]. All non-hydrogen atoms

were refined anisotropically, whereas the hydrogen atoms were place at a calculated position and refined in the final refinement.

Scanning Electron Microscope (SEM)

The morphologies of the synthesized VO_2-L metallogel were characterized using a scanning electron microscope (JSM-6360, Joel, with oxford EDS detector) operating at 1-30 kV. For sample preparation, diluted sample of VO_2-L metallogel was put into the thin aluminum sheet by using capillary tube and then allowing it to dry in air. The sample was also coated with a thin layer of Au before the experiment to minimize sample charging.

Procedure for synthesis of complex (VO_2-L)

A suspension of vanadium pentoxide (0.2 g, 1 mmol) in methanol solution was added dropwise to a methanol solution 20 ml containing the ligand (1 mmol). The reaction mixture was refluxed for 30 min at 70 °C. The reaction mixture was allowed to stand at room temperature, filtered, washed with warm methanol and dried to obtain the desired complex. Single crystal of complex was successfully obtained by slow evaporation of Water/DMF solution at ambient temperature. Colour: yellow; M.p: >300 °C; ^1H NMR (400 MHz, DMSO-d_6, Me_4Si): δ (ppm): 8.22-8.32 (d, 2H, H-C=N), 6.85-7.78 (m, 9H, Ar-H).

Typical procedure for the synthesis of VO_2-L Metallogel

In a typical gel formation reaction, a required amount of VO_2-L was dissolved in 2 mL of water/methanol (1:9; v/v) in a 5 mL vial and sonicated for 5 min to get a clear solution. The initial brown solution turned into either yellow or green. After that, the solution was kept undisturbed until the gel was formed. Then, the formation of gel was confirmed by the glass vial inversion method at room temperature (Scheme 2).

General experiment for oxidative bromination

In a 50 mL round bottom flask equipped with a magnetic stirring bar, substrates (10 mmol) were added. To this solution, KBr (40 mmol) dissolved in 20 mL water was added and then dissolved by stirring at ambient temperature followed by addition of a 15% H_2O_2 (4 mmol). The reaction mixture was stirred and VO_2-L metallogel (1 mmol) and 50% $HClO_4$ (4 mmol) were added at 0 °C for 10 minutes and then at 24 °C. An additional 4 mmol of 50 % $HClO_4$ was further added in three equal portions after every 10 minutes with continuous stirring. All the reactions were monitored using thin layer chromatography.

## Typical procedure for catalyst separation

At the end of every reaction, the aqueous solution was removed on a rotary evaporator. Then solid were washed with water to remove the VO_2-L metallogel, extracted

with CH$_2$Cl$_2$, dried over anhydrous MgSO$_4$ and then evaporated to afford the desired products. The NMR spectrum was recorded using the isolated product directly. The catalyst can be used for the next cycle of reactions without any decrease in products formation.

RESULTS AND DISCUSSION

Synthesis and characterization

The VO$_2$-L was synthesized by reaction of the ligand with vanadium pentoxide in 2:1 molar ratios in methanol (Scheme 1). VO$_2$-L is soluble in methanol, ethanol, acetonitrile, DMF and DMSO. Alternatively, VO$_2$-L was also synthesized using methanol/water as a solvent. The ^{1}H NMR spectral data of the ligand and VO$_2$-L were recorded using DMSO-d_6 and the data are given in the experimental section (Fig S7, S8). The ^{1}H NMR spectra of the ligand exhibits resonances at δ = 12.15 and 12.17 ppm which are assigned to -OH proton attached to phenyl ring, the signal at δ = 11.45 is assigned to -NH proton, both these peaks disappeared upon complexation, confirming the ligand coordinate to metal ions in deprotonated form. The aromatic proton appeared at the expected position in the ranges δ = 6.85-8.32 ppm.
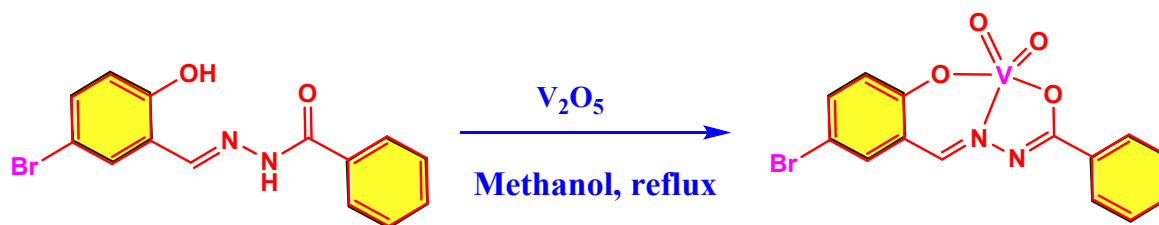
Scheme 1. Schematic diagram showing the preparation of VO$_2$-

Molecular structure

The molecular structure of VO$_2$-L was determined by Single Crystal X-ray crystallography (Fig 1). The crystal data and structure refinement parameters for VO$_2$-L are given in Table 1. Selected bond lengths and bond angles are presented in Table 2. VO$_2$-L crystallized in monoclinic P2$_1$/c space group. The ligand coordinates to metal ion in tridentate fashion through -ONO- donor atom at the basal position, together with two oxido ligand at the terminal position forming penta-coordinate geometry around the metal center. The metal bond distances in VO$_2$-L are 1.889(9) Å (V1-O1), 1.957(8) Å (V1-O2), 1.648(7) Å (V1=O3), 1.571(8) Å (V1=O4), 1.884(9) Å (V2-O5), 1.961(8) Å (V2-O6), 1.661(8) Å (V2=O7), 1.562(8) Å (V2=O8), 2.128(10) Å (V1-N1) and 2.117(9) Å (V2-N3). The geometrical bond angles around the vanadium ions are 73.9(3)° (O2-V1-N1), 91.8(4)° (O3-V1-O2), 96.0(4)° (O3-V1-O1), 144.2(4)° (O3-V1-N1), 149.0(4)° (O1-V1-O1), 82.5(4)° (O1-V1-N1), 105.7(4)° (O4-V1-O2), 107.6(5)° (O4-V1-O3), 100.4(5)° (O4-V1-O1), 107.7(4)°

(O4-V1-N1), 91.5(4)° (O7-V2-O6), 96.3(4)° (O7-V2-O5), 142.0(4)° (O7-V2-N3), 74.1(4)° (O6-V2-N3), 108.4(5)° (O8-V2-O7), 103.9(5)° (O8-V2-O6), 100.1(5)° (O8-V2-O5), 109.2(4)° (O8-V2-N3), 150.9(4)° (O5-V2-O6) and 82.8(4)° (O5-V2-N3). Their geometrical trans angle in VO$_2$-L are 144.2(4)° (O3-V1-N1) and 149.0(4)° (O1-V1-O2) around V1, and 142.0(4)° (O7-V2-N3) and 150.9(4)° (O5-V2-O6) around the vanadium ion (V2). Their corresponding geometrical index are $\tau_1 = 0.08$ and $\tau_2 = 0.15$. Hence, vanadium atom adopted a distorted square pyramidal geometry with slight distortion.
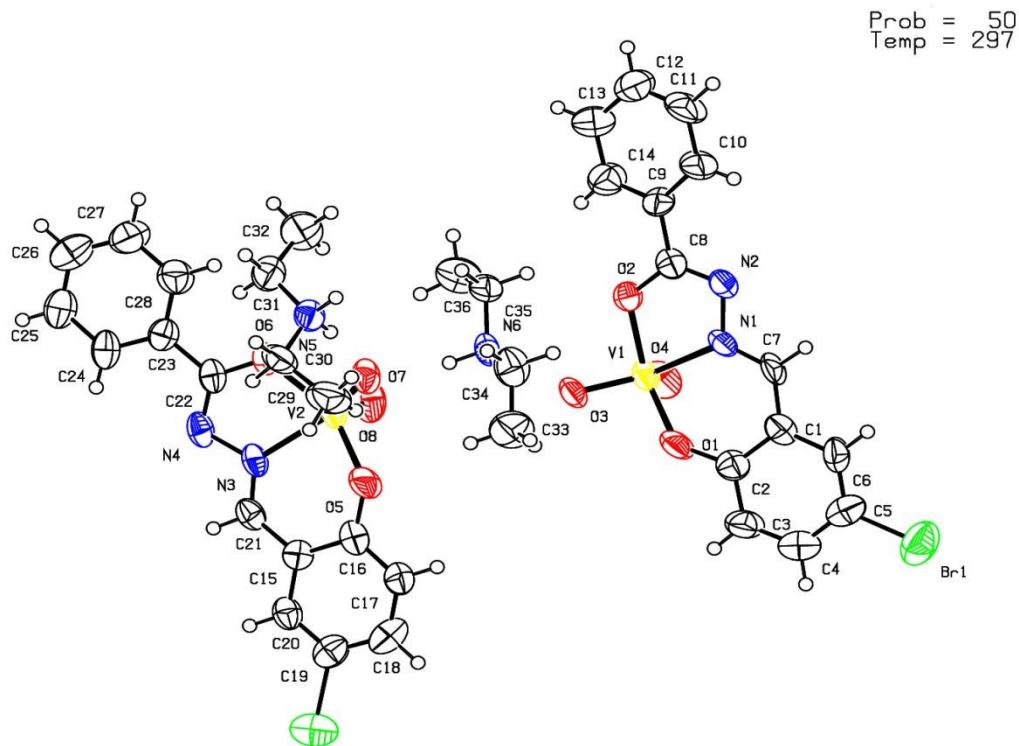

Fig 1. ORTEP diagram of VO$_2$-L with 50% probability

Table 1. Crystal data and structure refinement

Empirical formula	C$_{18}$H$_{21}$BrN$_3$O$_4$V
Formula weight	474.23
Temperature/K	297.3(5)
Crystal system	monoclinic
Space group	P2$_1$/c
a/Å	8.371(3)
b/Å	22.101(10)
c/Å	22.370(14)
α/°	90
β/°	90
γ/°	90
Volume/Å^3	4138(4)
Z	8
ρ$_{calc}$g/cm^3	1.522

Radiation   Mo K α (λ = 0.71073)

Reflections collected   12650

Data/restraints/parameters 7238/0/491

Goodness-of-fit on F^2 1.057

Final R indexes [I>=2σ (I)] $R_1 = 0.1055$, $wR_2 = 0.2495$

Final R indexes [all data] $R_1 = 0.1943$, $wR_2 = 0.2975$

Table 2. Selected experimental parameters obtained by X-ray crystallography and calculated

for VO_2-L

Parameters	Experimental	Theoretical (B3LYP)		
		6-31G+(d, p): LANL2DZ	6-31G+(d, p): LANL2MB	6-31G+(d, p): SDD
Bond lengths				
V1-O1	1.889(9)	1.898	1.919	1.895
V1-O2	1.957(8)	2.078	2.096	2.079
V1-O3	1.648(7)	1.614	1.641	1.602
V1-O4	1.571(8)	1.618	1.632	1.598
V1-N1	2.128(10)	2.248	2.231	2.274
Bond angles				
O2-V1-N1	73.9(3)	71.606	71.875	71.032
O3-V1-O2	91.8(4)	92.022	98.823	92.640
O3-V1-O1	96.0(4)	101.279	106.103	101.617
O3-V1-N1	144.2(4)	143.034	148.283	146.149
O1-V1-O2	149.0(4)	145.833	144.683	142.807
O1-V1-N1	82.5(4)	79.164	79.528	78.416
O4-V1-O2	105.7(4)	98.407	92.113	99.682
O4-V1-O3	107.6(5)	110.132	110.055	110.496
O4-V1-O1	100.4(5)	106.060	102.108	106.907
O4-V1-N1	107.7(4)	105.029	99.568	101.570
Dihedral angle				
N2-N1-C7-C1	177.7(10)	179.213	177.464	179.113
N1-N2-C8-C9	-178.0(10)	-179.812	-179.341	-179.846
O2-C8-C9-C10	173.2(11)	167.233	169.940	165.314
N1-C7-C1-C6	-178.6(12)	-177.427	-176.818	-177.411
C6-C1-C2-O1	172.5(11)	177.878	178.195	177.709
O1-C2-C3-C4	-174.4(13)	-178.642	-178.642	-178.197
C7-N1-N2-C8	179.2(10)	177.915	179.925	178.530
V1-O2-C8-C9	171.8(8)	172.841	171.327	170.754
V1-O2-C2-C3	-155.4(10)	-154.966	-155.597	-151.758

Molecular packing diagram

The molecular packing involves C-H---O, N-H---O hydrogen bonding interaction and

pi-pi stacking between the aromatic rings. The combined effect of which is to form a layer

structure parallel ladder like structure. The N-H---O molecular synthon are parallel to each

other on both side of pi-pi stacking forming as zig-zag 1D dimensional arrangements (Fig

2A). Moreover, the presence of weak halogen bonding (Br…Br) generates a self-assembly molecular structure in the structural unit of the VO_2-L (Fig 2B). The diethyl-ammonium hydrogen provides a crosslink by acting as a donor toward the Oxido-ligand bonded to vanadium ions. The bond lengths are N(5) --H(5A) ..O(7) 2.761(12) Å, N(5) --H(5B) ..O(3) 2.770(12) Å, N(6) --H(6A) ..O(3) 2.733(12) Å, N(6) --H(6A) ..O(3) 2.733(12) Å and N(6) --H(6B) ..O(7) 2.752(11) with geometrical bond angle between the donor and acceptor 171°, 153°, 165° and 160°. The distances between the two aromatic rings forming pi-pi stacking interaction is 3.786 Å and Br…Br interaction is 3.578 Å.
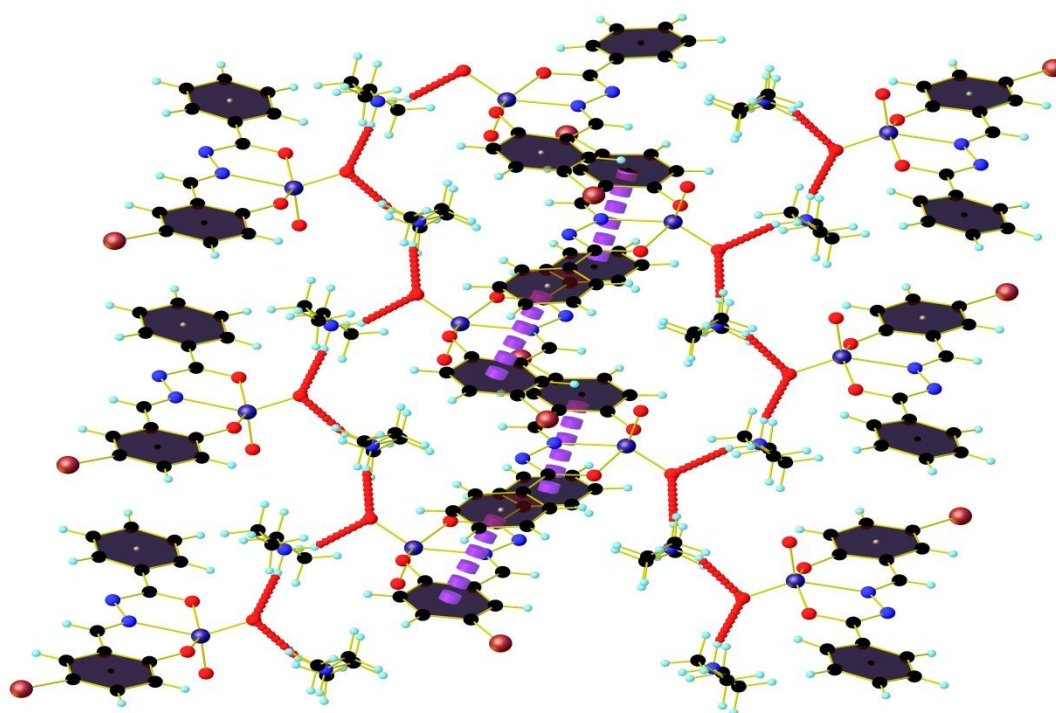
Fig 2A. Zig-zag 1D dimensional arrangements and ladder like structure connected through hydrogen bonding interaction and pipi-stacking.
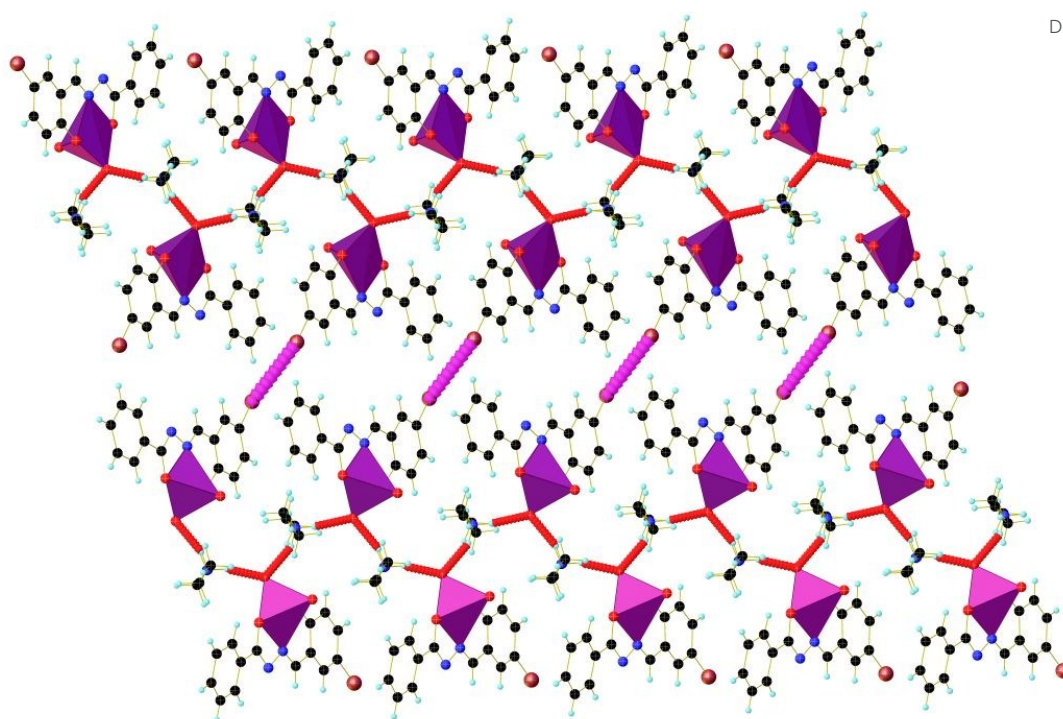
Fig 2B. Supramolecular self-assembly form through hydrogen bonding and weak halogen bonding interaction (Br…. Br).

Computational studies

Theoretical studies were performed in gas phase using Density functional theory (DFT) with hybrid functional B3LYP with different basis set for metal ions (LANL2DZ, LANL2MB and SDD) and 6-31+G(d,p) basis set for carbon, hydrogen, oxygen, nitrogen and bromine atoms implemented in using GAUSSIAN 09 program [35]. The geometrical bond lengths and bond angles of the optimized structures using different basis set are presented in Table 2. The theoretical bond lengths are 1.895-1.919 Å (V1-O1), 2.078-2.096 Å (V1-O2), 1.602-1.641 Å (V1-O3), 1.598-1.632 Å (V1-O4) and 2.231-2.274 Å (V1-N) with geometrical trans angles 143.034-148.283° (O3-V1-N1), 142.807-145.833° (O1-V1-O2). The calculated torsion angles are 177.464 - 179.213° (N2-N1-C7-C1), 165.314 - 169.940° (O2-C8-C9-C10), -176.818 - -177.427° (N1-C7-C1-C6). Hence, the experimental geometrical parameters and theoretical results show satisfactory agreement. As can be seen from the bond lengths and bond angles the results obtained from theoretical slightly different from the experimental ones. Thus, most of the calculated parameters are slightly higher compared experimental values. It can be noted that the theoretical results depend on the isolated gaseous state, whereas in solid state the presence of inter molecular interactions connected the molecules together, which results in the differences of geometrical bond lengths and bond angles between the experimental and the calculated values [36]. The charge distributions of VO$_2$-L

are given in Table 3, whereas the contour plot for highest occupied molecular orbital (HOMO) and the lowest unoccupied molecular orbital (LUMO) are presented in Fig 3. The charged distribution shows that the carbon atom attached to electronegative atoms such as nitrogen and oxygen are positive, whereas oxygen, nitrogen and other carbon atoms are negative. The computed charged for metal ions using different basis sets are 0.709, 0.773 and 1.539, which are lower than the expected formal charged of +5. The difference arises due to significant electron transfer process involved from the donor atoms such as O_{oxo}, $O_{phenoxo}$ and nitrogen (azomethine) towards central metal ions. Similarly, the central metal atom has d^0 electronic configuration but orbital occupations shows that the population state of d_{xy}, d_{xz}, d_{yz}, $d_{x^2-y^2}$ and d_{z^2} are 0.581, 0.605, 0.666, 0.552 and 0.715, respectively. These results provide evidence about the electron transfer involved from donor atoms toward metal ion.
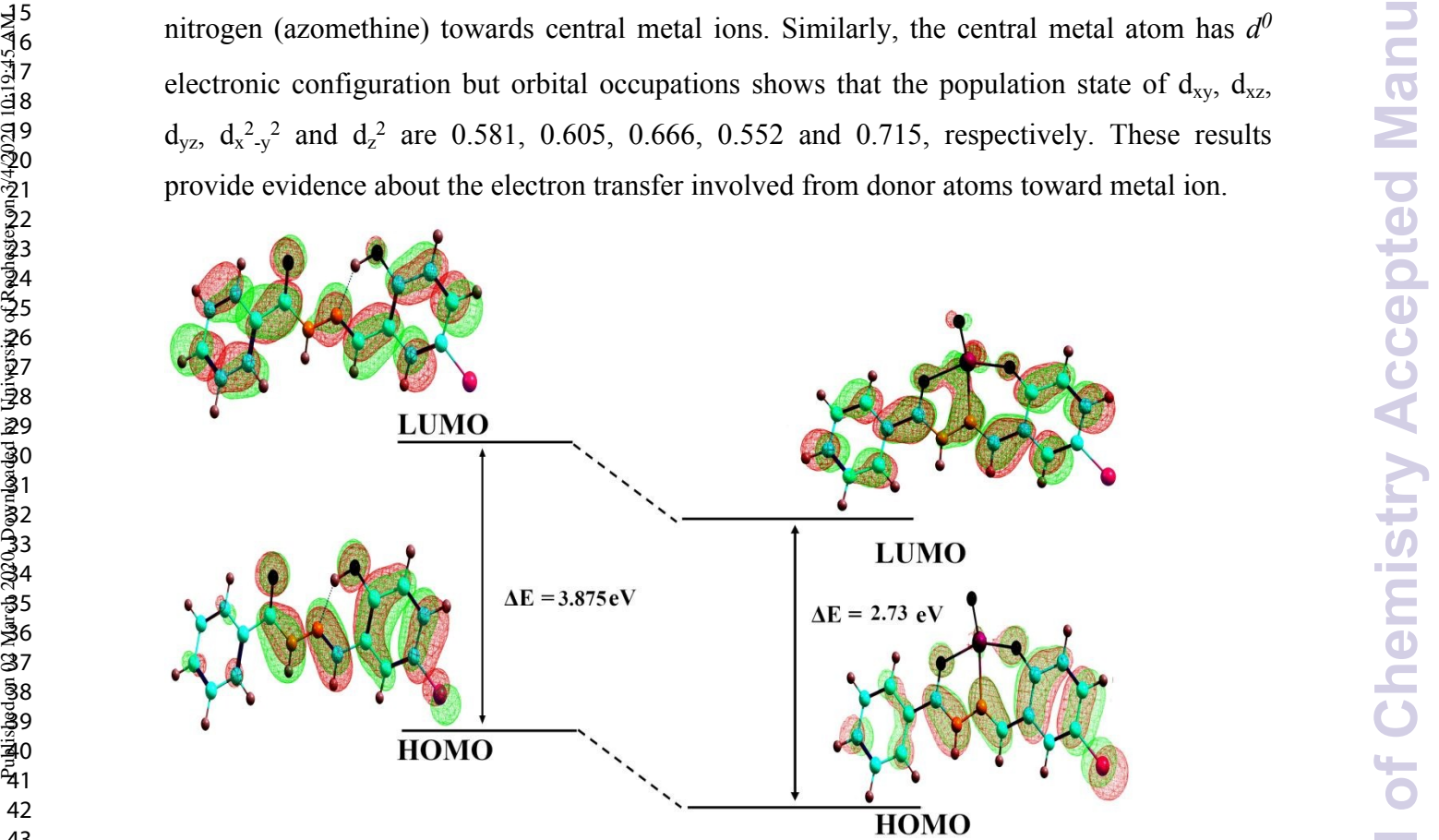

Fig 3. Contour plots for some selected molecular orbitals of ligand and VO_2-L along with their relative energies of HOMOs (lower orbitals) and LUMOs (upper orbitals).

Table 3. Selected Mulliken atomic charges of ligand and VO_2-L

Atom	Ligand: 6-31G+(d, p)	6-31G+(d, p): LANL2DZ	6-31G+(d, p): LANL2MB	6-31G+(d, p): SDD
O1	-0.712	-0.568	-0.701	-0.562
O2	-0.596	-0.537	-0.637	-0.533
N1	-0.291	-0.298	-0.371	-0.294
N2	-0.461	-0.411	-0.416	-0.408
Br	0.037	0.05209	0.051	0.052
V	-	0.77283	1.539	0.709

Gelation studies

From single crystal structure analysis, we noticed that the VO_2-L metallogel exhibits pi-pi interaction and weak hydrogen bonding. Moreover, apart from these interactions, the VO_2- metallogel displays weak non-covalent interaction. Encourage by these structural properties possessed by VO_2-L we carried out gelation experiments. The gelation experiments of VO_2-L were carried out using "stable to inversion of a test tube" method in various solvents such as water, methanol, ethanol, acetonitrile, chloroform, toluene, DMSO, DMF, water/methanol etc. Thus, after several attempts and by changing the solvents, gelation in water/methanol (1:9 (v/v) ratios) was observed. We also carried out, a control experiment to test the gelation behaviour of the VO_2-L metallogel and found that it could also gel in water/methanol (1:9 (v/v) ratios) and the gelation behaviour of the VO_2-L (1:9 (v/v) ratios) was thermo-reversible. The VO_2-L metallogel exhibits excellent gelation abilities and turned out to be quite efficient displaying 1.3 wt % minimum gelator concentration, with gel-sol dissociation temperature T_{gel}, of 58 °C (water/methanol) measured by using the 'tilted tube' method (Fig 4).
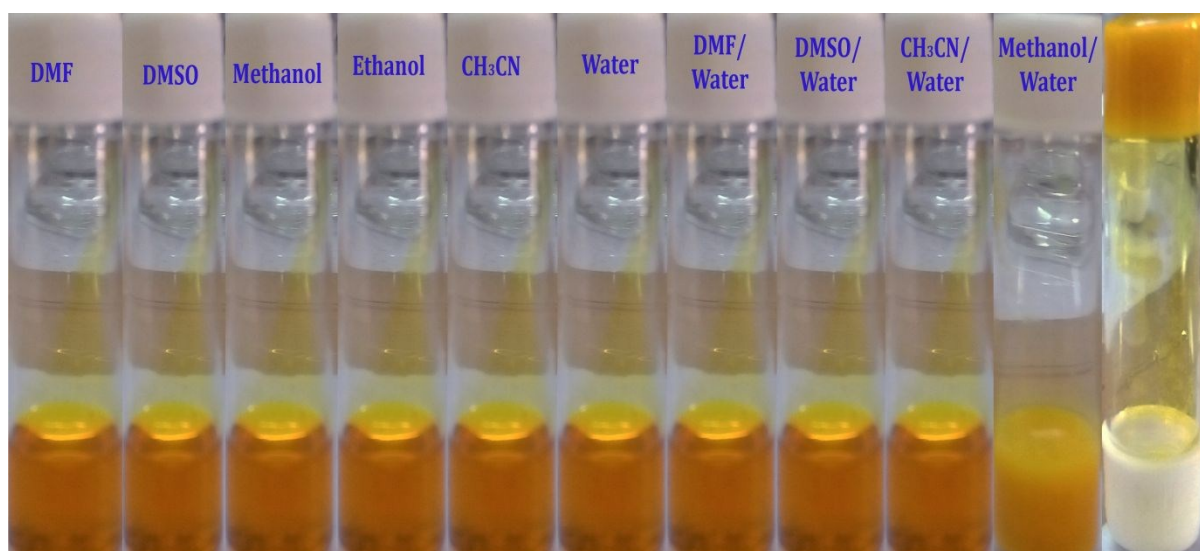

Fig 4. Gelation test carried out using different solvents combination

During the metellogel formation, various interactions present in the structural units and crystal lattice of the VO_2-L metallogel such as, non-covalent interaction and pi-pi stacking interactions between aromatic rings might have played crucial roles and act in tandem to stabilize the gel structure. It may also be noted that the hydrogen bonding between solvents molecules and gelator is very importance for molecular self-assembly required for gelation. FT-IR spectroscopy was performed to identify the nature of participation of functional groups present in the ligand and in their corresponding metallogel. The ligand

exhibits a broad band at 3448, 3270 and 1663 cm^{-1} which are assigned to the phenolic-OH and C=O group. Whereas, VO$_2$-L metallogel the peaks at 3448, 3270 and 1663 cm^{-1} were not observed, indicating that the ligand coordinated to metal ions in deprotonated form. VO$_2$-L metallogel shows a strong band at 1525 cm^{-1} and is assigned newly NCO-group. However, the IR spectrum of VO$_2$-L metallogel show new band at 587 cm^{-1} and 487cm^{-1}. These bands can be assign to v(M-O)(phenolic) and v(M-O)(carbonyl), respectively. The VO$_2$-L metallogel exhibit strong bands in the range 909-941 cm^{-1} and are assigned to V=O vibrations. These observations were consistent with that obtained from the IR performed with the crystalline form. Moreover, the morphological features of the gel were studied using SEM which shows a porous morphology inherited void space in the interlaced gel matrix (Fig. S11). The smaller particles packed up together into larger particles, with pores in between and tend to remain in the most thermodynamically favourable state. These small particles upon aggregation form larger particles which further form typical metallogel architecture. The presence of H-bonding and p-p stacking in gel are supported by single X-ray diffraction. The experimental XRD patterns of the xerogel are in good agreement with simulated XRD patterns from single crystal X-ray diffraction results as shown in Fig. S9. The simulated pattern of the VO2-L was calculated from single crystal structure data (cif) using CCDC Mercury software. In order to understand the stiffness of aggregation, rheological measurement of the gel was also studied. The plot of elastic modulus (G′) and viscous modulus (G″) against sheer stress at a constant frequency of 1 Hz are shown in Fig. S10a and Fig. S10b. The plot shows that above a critical stress, G′ and G″ decreases. The critical stress, i.e. yield stress of the hydrogel, was found to be of about 312 Pa indicating its high mechanical strength. During the measurement, it was observed that elastic modulus (G′) and viscous modulus (G″) are almost parallel to the frequency imposed. This confirms that the material switches to the true gel state and results agree well with classical gels.

Stimuli-Responsive Metallogel

Stimuli responsive behaviors of supramolecular metallogels to various physical factors such as light, temperature, sound and force are known up to date. Similarly, the responsive behavior of these metallogels are not only restricted to physical factors but to chemical factors, stimuli toward ligand, pH and anions. Subsequently, the responsive properties of VO$_2$-L metallogel toward ions and molecules were investigated. In the first case the ions sensing properties was investigated by adding and permeating various anions such as F$^-$, Br$^-$, I$^-$, CN$^-$, HSO$_4^-$, ACO$^-$, H$_2$PO$_4^-$, ClO$_4^-$, N$_3^-$ and OH$^-$ into VO$_2$-L metallogel. As shown

in Fig 5B, VO$_2$-L metallogel displayed blue colour fluorescence upon addition of OH$^-$ anions. The fluorescence intensity enhances gradually and showed a maximum emission peak at 475 nm (Fig 5A). Therefore, VO$_2$-L metallogel could sense OH$^-$ anions with specific selectivity. From the fluorescence titration profile, the association constant was found to be 1.68×10^4 M^{-1}, calculated using Benesi-Hildebrand plot. Hence, the detection limit of VO$_2$-L metallogel for OH$^-$ was 1.78×10^{-8} mL^{-1} which was obtained from fluorescence titration (Figure 5C) and indicates high detection sensitivity for OH$^-$ anions.
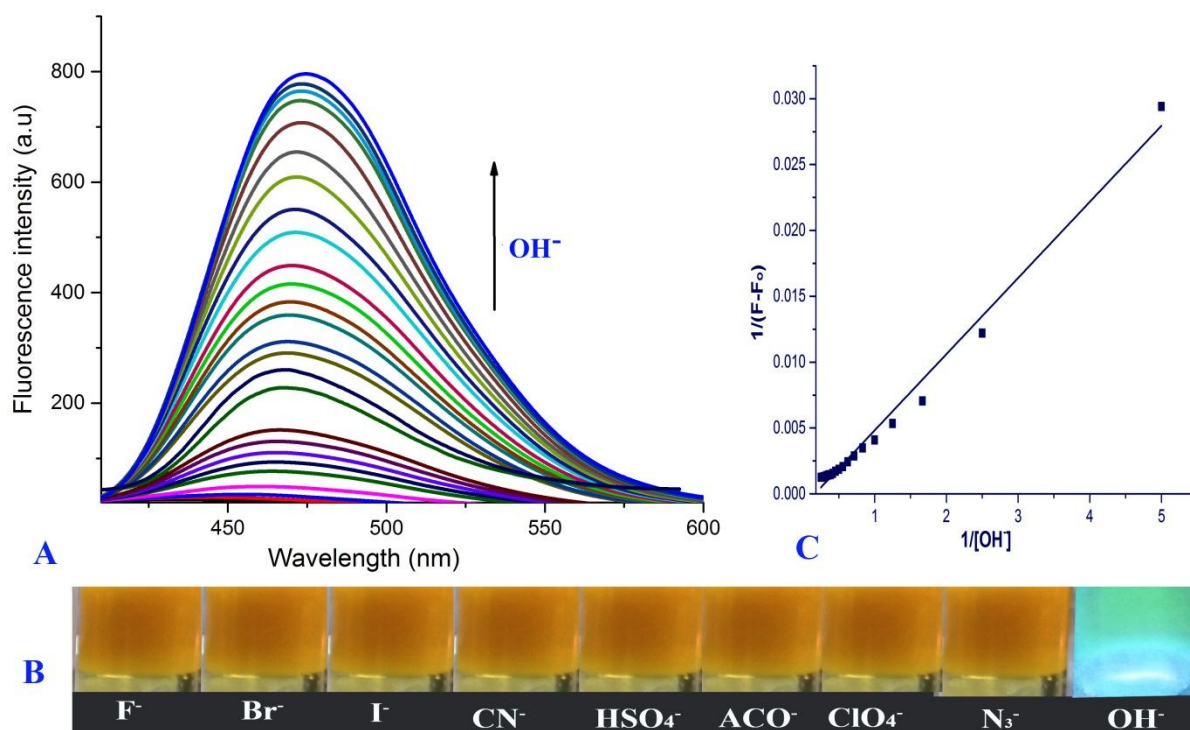
Fig 5. Fluorescence spectra of (A) VO$_2$-L metallogel with increasing concentrations of OH$^-$ (B) Fluorescence responses of VO$_2$-L metallogel in the presence of various anions (C) Benesi-Hildebrand plot for calculating the association constant.

We also introduced various metal ions by adding and diffusing into VO$_2$-L metallogel, including Na$^+$, K$^+$, Cs$^+$, Mg^{2+}, Ca^{2+}, Cr^{3+}, Fe^{3+}, Co^{2+}, Ni^{2+}, Cu^{2+}, Zn^{2+}, Ag$^+$, Cd^{2+}, Hg^{2+} and Al^{3+}. The addition of these metal cations does not display any fluorescence properties. The reactivity of VO$_2$-L metallogel toward other molecules such as HCl and H$_2$O$_2$ were also carried out. During the addition of HCl the VO$_2$-L metallogel collapse and show light yellow color solution without retaining its original shape, whereas during the addition of hydrogen peroxide the color of the gel turn to red color solution (Fig 7). Further evidence of this transition was obtained by measuring UV-vis spectral changes (Fig. 6A). It was observed that the absorption band at 392 nm is the characteristic of ligand to metal charge transfer (MLCT). Addition of H$_2$O$_2$ (1 equivalent) to the gel solution increases the band intensity at

280 nm, whereas the absorption band at 392 nm decreases its intensity, respectively. Further, after addition of the H_2O_2 solution, a new band at 330 nm appeared and two isosbestic points at 347 nm and 320 nm was observed. The results obtained may be interpreted due to the formation of peroxovanadium species [33]. During the course of the reaction the solution changes it colour from yellow to red. Hence, VO_2-L metallogel can be used for colorimetric detection of hydrogen peroxide. Similarly, reaction of VO_2-L metallogel with HCl were also studied using UV/Vis spectroscopy (Fig 6B). During the addition of an acid to the gel solution (HCl, 1 equivalent), the band at 312 nm increases its intensity, whereas the absorption band at 392 nm decreases its intensity with the presence of two isosbestic point at 360 nm and 425 nm. Hence, these results obtained correspond to the formation of oxo-hydroxo species as reported in the literature [34].
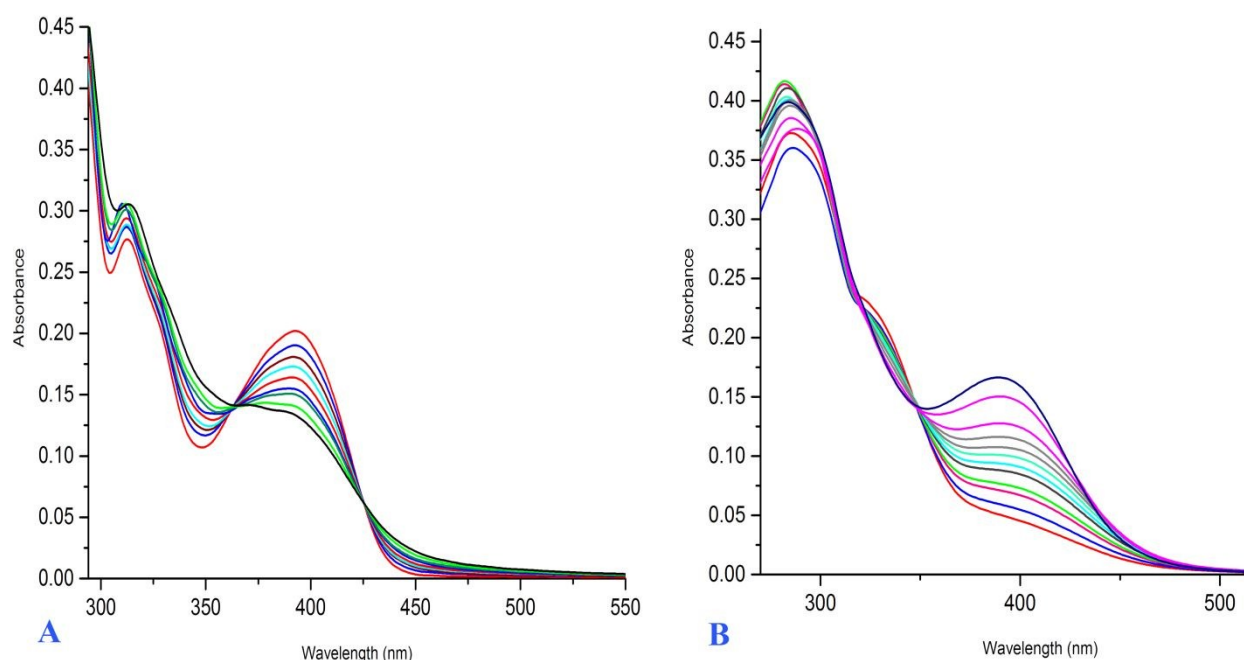
Fig 6. Spectral changes observed during the reaction VO_2-L metallogel with (A) HCl and (B) H_2O_2
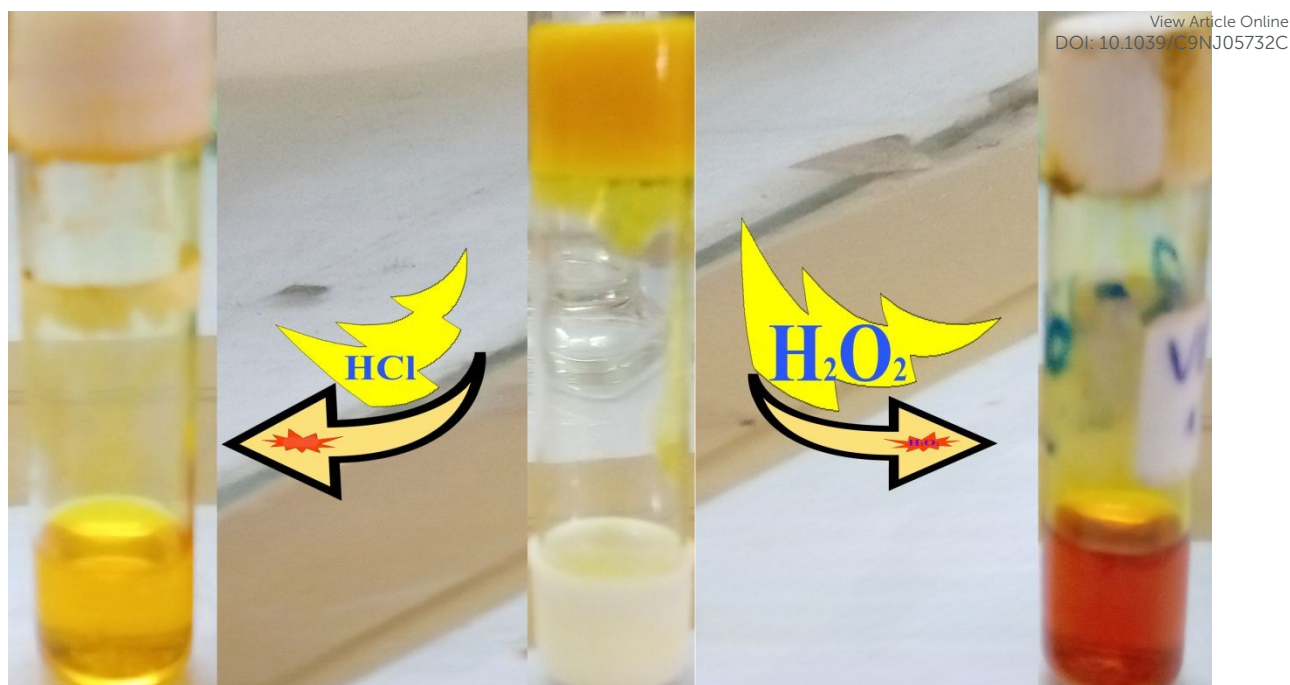
Fig 7. Reaction of VO$_2$-L metallogel towards hydrochloric acid and hydrogen peroxide

Bromoperoxidase-like activity

In this article, we also explore the catalytic studies for oxidative bromination of some organic substrates using solid state structure and gel form. To achieve the best optimum condition for oxidative bromination reactions, we carried out the reaction using phenol red as the model substrate (Table S1). Using VO$_2$-L metallogel, as the pre-catalyst, the reaction was tested at different amounts of catalyst/substrate ratios and it was found that 1:10 molar ratios of VO$_2$- metallogel /substrates gave the optimum yield. Using VO$_2$-L metallogel /substrate 1:10 molar ratios, the effect of bromides sources was also studied and found that VO$_2$-metallogel /substrate/KBr in 1:10:40 molar ratios gave the best yield. The effect of hydrogen peroxide was also evaluated and found that 1:10:40:40 molar ratios of VO$_2$-L metallogel /substrate/KBr/hydrogen peroxide gave the maximum yield. The effects of acid for the oxidative bromination reaction were also studied and it was found that 4 molars of HClO$_4$ gave maximum yield (Table S1, entry 11). From the above studies, we concluded that the present of acid is essential for catalytic bromination reaction. The oxidative bromination reaction were also carried out using different vanadium species such VOSO$_4$, V$_2$O$_5$, NaVO$_4$ and vanadyl acetylacetonate, but it was found that VO$_2$-L metallogel gave the high yield. Similarly, the reactions were also carried out in wide varieties of solvents and it was found that the reaction proceeds smoothly in aqueous solution.

Therefore, in order to test the versatility of the catalyst, we carried out the catalytic oxidative bromination reaction using various organic substrates. Some of the selected results
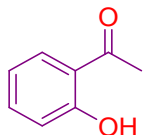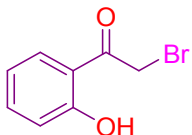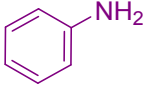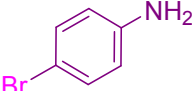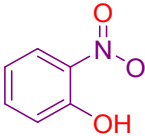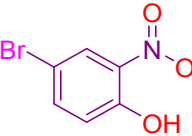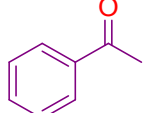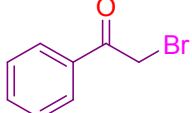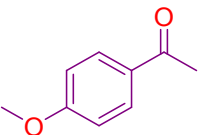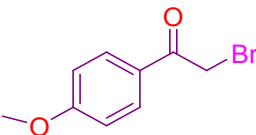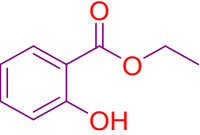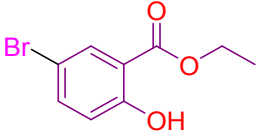
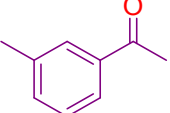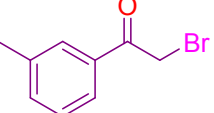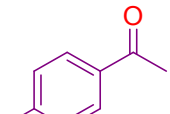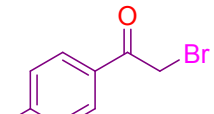are listed in Table 4. The bromination reaction of phenol red gave 89% yield of the product phenol blue within 45 min and salicylaldehyde gave 90% yield of 5-bromo salicylaldehyde in 40 min (Table 4, entry 1, 2). Bromination reaction of aniline was also carried out successfully giving p-bromoaniline with 87% yield as the only product within 30 min (Table 4, entry 4). The reactions were also carried out using 2-nitro phenol and ethyl salicylate as the substrates giving the product 5-bromo-2-nitro phenol with 90% yield and 5-bromoethyl salicylate with 86% yield as the brominated product (Table 4, entry 5, 8). Inspired by these results, we hypothesized that the α-bromoketone might be obtained using VO$_2$-L metallogel and acetophenone as the substrate. In our study, we found that bromination of acetophenone gave α-bromoacetophenone as the only product with 88% yield within the time period of 35 min (Table 4, entry 6). In order to widen the substrates scope bromination reaction of different substituted α-bromoketone was also carried out, such as 2-hydroxy acetophenone gave the product α-bromo-2-hydroxy acetophenone with 85% yield within 25 min (Table 5, entry 3) lower than that of unsubstituted acetophenone. Bromination reaction of p-methoxy-acetophenone gave the product α-bromo-p-methoxy-acetophenone with 90% yield in 30 min, higher yield is due to the electron donating nature of methoxy group present in the para position of the benzene ring (Table 4, entry 7). Other substituted ketones such as 4-methyl-2-hydroxy- acetophenone and 5-methyl-2-hydroxy- acetophenone were also smoothly mono-brominated to α-bromoketone in high yields (90-93%, Table 4, entry 9, 10). The present catalytic approach provides efficient and simple access to α-bromoketones.
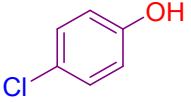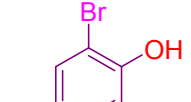
Table 4. Self-assembled metal-organic metallogel catalyzed oxidative bromination under mild condition

1a → 2a, 89%
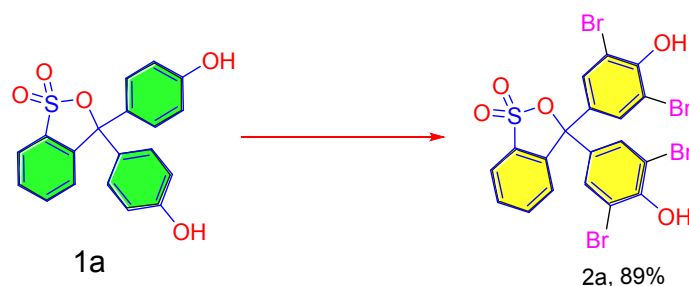
Entry	Alcohol	Product	Time (min)	Yield (%) (isolated)	TON	TOF (min^{-1})
1	1b		40	90	900	22.5

	1	2 **2b**				
2	**1c**	**2c**	25	85	850	34
3	**1d**	**2d**	30	87	870	29
4	**1e**	**2e**	40	90	900	22.5
5	**1f**	**2f**	35	88	880	25.14
6	**1g**	**2g**	30	90	900	30
7	**1h**	**2h**	35	86	860	24.57
8	**1i**	**2i**	40	91	910	22.75
9	**1j**	**2j**	40	93	930	23.25

10	1k	2k	34	91	910	26.76

We also carried out a standard reaction or controlled experiments in which VO_2-L is used as catalyst and p-methoxy-acetophenone as a substrate. VO_2-L catalysed the oxidative bromination of p-methoxy-acetophenone and gave α-bromo-p-methoxy-acetophenone as the only product with 78% yield in 45 min. Therefore, the results obtained shows that VO_2-L metallogel act as a better catalyst and gave the high yield compared simple vanadium complex (VO_2-L). **Based** on the above studies, we proposed the following mechanism highlight in scheme 1. VO_2-L metallogel on dissolution with 15% H_2O_2 gives rise to the formation of peroxo species. In sufficiently acidic condition bromides is oxidized forming HOBr, Br_3^-, Br_2^- or V-OBr species. Oxidation of bromide by hydrogen peroxide in aqueous solution is only thermodynamically feasible under acidic or neutral condition. In the final step the oxidized bromide species is then trapped by organic substrates to give brominated products as shown in Scheme 2.
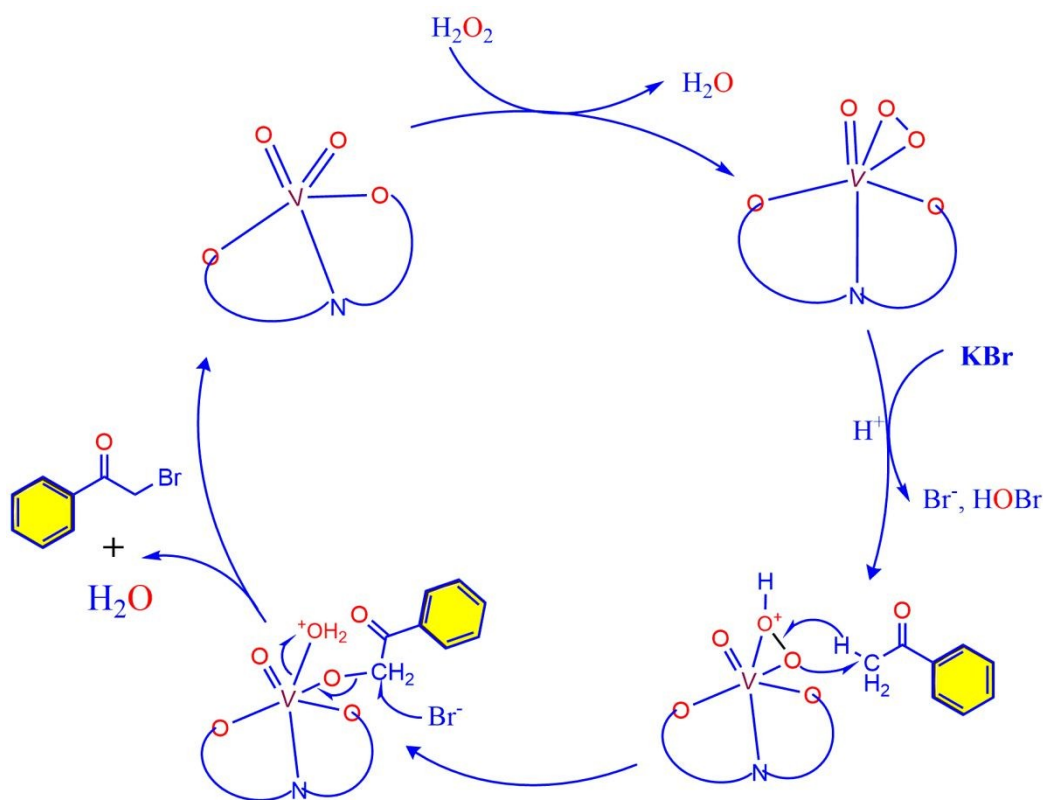
Scheme 2. Possible mechanism for the catalytic studies

CONCLUSIONS

We have developed a novel and efficient protocol for oxidative bromination of some organic substrates using simple VO$_2$-L metallogel as catalyst. The process is appreciable due to safety, simplicity, availability and cheapness of the VO$_2$-L metallogel. The whole protocols involved are very simple and operates under mild conditions, which makes the present procedure very attractive and prospective. Hence, VO$_2$-L metallogel catalysed the peroxidative bromination of phenol, phenol derivatives and other organic substrates and its act as a potential functional model of vanadium enzymes haloperoxidases.

ACKNOWLEDGEMENTS

REFERENCES

1 D. Wischang, O. Brucher and J. Hartung, *Coord. Chem. Rev.,* 2011, **255**, 2204–2217.

2 J. A. L. da Silva, J. J. R. Frausto da Silva and A. J. L. Pombeiro, *Coord. Chem. Rev.*, 2011, **255**, 2232-2248.

3 A. Podgorsek, M. Zupan and J. Iskra, *Angew. Chem. Int. Ed.*, 2009, **48**, 8424.

4 K. Kikushima, T. Moriuchi and T. Hirao, *Tetrahedron.*, 2010, **66**, 6906.

5 V. Kavala, S. Naik and B. K. Patel, *J. Org. Chem*., 2005, **70**, 4267.

6 S. Adimurthy, G. Ramachandraiah, A.V. Bedekar, S. Ghosh, B. C. Ranu and P. K. Ghosh, *Green Chem.*, 2006, **8**, 916.

7 G. Majetich, R. Hicks and S. Reister, *J. Org. Chem*., 1997, **62**, 4321.

8 R. E. Buckles, R. C. Johnson and W. J. Probst, *J. Org. Chem*., 1957, **22**, 55.

9 G. Grivani, V. Tahmasebi and A. Dehno Khalaji, *Polyhedron*., 2014, **68**, 144–150.

10 A. Podgoršek, M. Eissen, J. Fleckenstein, S. Stavber, M. Zupan and J. Iskra, *Green Chem.* 2009.**, 11**, 120.

11 V. Nair, L. Balagopal, R. Rajan and J. Mathew, *Acc. Chem. Res.*, 2004, **37**, 21-30.

12 G. I. Nikishin, N. I. Kapustina, L. L. Sokova, O. V. Bityukov and A. O. Terentev, *Tetrahedron Lett*., 2017, **58**, 352-354.

13 G.-W. Wang and J. Gao, *Green Chem.,* 2012, **14**, 1125.

14 H. A. Muathen, *Synth Commun.,* 2004, **34**, 3545-3552.

15 L. Kumar, T. Mahajan and D. D. Agarwal, *Ind. Eng. Chem. Res.* 2012, **51 (36)**, 11593-11597.

16   M. M. Cummings and B.C.G. Sunderberg, *Synth Commun.,* 2014, **44**, 954-958.

17   A. Butler, *In Comprehensive Biological Catalysis*; M. Sinnott, Ed., British Academic
      Press, Oxford, U. K. 1997, 427.

18.   A. Butler, In Bioinorganic Catalysis; J. Reeddijk, Eds.; *Marcel Dekker*; New York,
      1993, 424.

19   M. I. Isupov, A. R. Dalby, A. M. Brindley, Y. Izumi, T. Tanabe, G. N. Murshudov and
      J. A. Littlechild, *J. Mol. Biol.*, 2000, **299**, 1035.

20   C. Das, P. Adak, S. Mondal, R. Sekiya, R. Kuroda, S. I. Gorelsky and S. K.
      Chattopadhyay, *Inorg. Chem.,* 2014, **53**, 11426–11437.

21   M. R. Maurya, N. Chaudhary and F. Avecilla, *Polyhedron.,* 2014, **67**, 436–448.

22   V. Conte and B. Floris, *Inorg. Chim. Acta.,* 2010, **363**, 1935.

23   U. Bora, G. Bose, M. K. Chaudhuri, S. S. Dhar, R. Gopinath, A.T. Khan and B. K.
      Patel, *Org. Lett.*, 2000, **2**, 247.

24   V. Conte, B. Floris, P. Galloni and A. Silvagni, *Pure Appl. Chem.*, 2005, **77**, 1575.

25   B. F. Sels, D. E. De Vos, M. Buntinx and P. A. Jacobs, *J. Catal.*, 2003, **216**, 288.

26   B. M. Choudary, T. Someshwar, M. L. Kantam, Reddy and C. V. *Catal. Commun.*,
      2004, **5**, 215.

27   J. H. Espenson, O. Pestovsky, P. Huston and S. Staudt, *J. Am. Chem. Soc.*, 1994, **116**,
      2869.

28   L. Yang, Z. Lu and S. S. Stahl, *Chem. Commun.,* 2009, 6460.

29   A. Podgorsek, M. Zupan and J. Iskra, *Angew. Chem., Int. Ed.*, 2009, **48**, 8424–8450.

30   (a) W. Fang, Y. Zhang, J. Wu, C. Liu, H. Zhu and T. Tu, *Chem.–Asian* J., 2018, 13,
      712–729; (b) B. Escuder, F. Rodriguez-Llansola and J. F. Miravet, *New J. Chem.*, 2010,
      34, 1044–1054.

31.   G. M. Sheldrick, SADABS Program for Empirical Absorption Correction of Area
      Detector Data University of Göttingen Göttingen, Germany, 1996.

32   G. M. Sheldrick, SHELXL-14 Program for Crystal Structure Refinements University of
      Gottingen Gottingen, Germany, 1996.

33   S. D. Kurbah, I. Syiemlieh and R. A. Lal, *R. Soc. open sci.*, 2018, **5**, 171471.

34   M. R. Maurya, S. Agarwal, C. Bader, M. Ebel and D. Rehder, *Dalton Trans.*, 2005,
      537-544.

35   M. J. Frisch and G. W. Trucks, et.al.; GAUSSIAN 09 Revision C.01 Gaussian Inc
      Walling-ford CT, 2009.

36   F. F. Jian, P. S. Zhao, Z. S. Bai and L. Zhang, *Struct. Chem.*, 2005, **16**, 635.